Structural Engineering and Mechanics, *Vol. 70, No. 5 (2019) 591-600*
DOI: https://doi.org/10.12989/sem.2019.70.5.591

The cyclic behavior of steel-polyoxymethylene composite braces

Serhat Demir*

Department of Civil Engineering, Karadeniz Technical University, Trabzon, Turkey

(Received February 6, 2019, Revised March 6, 2019, Accepted March 8, 2019)

Abstract. Steel tubular buckling controlled braces are well known as being simple, practical and cost-effective lateral force resisting systems. Although these system features have gained the attention of the researchers over the last decade, steel tubular buckling controlled braces currently have limited application. Indeed, only a few steel tubes tightly encased within each other exist in the steel industry. In this paper, a new and practical design method is proposed in order to better promote the widespeared application for current steel tubular buckling controlled brace applications. In order to reach this goal, a holed-adapter made with polyoxymethylene adaptable to all round and square steel sections, was developed to use as infiller. The research program presents designing, producing and displacement controlled cyclic loading tests of a conventional tubular brace and a buckling controlled composite brace. In addition, numerical analysis was carried out to compare the experimental results. As a result of the experimental studies, buckling was controlled up to 0.88 % drift ratio and the energy dissipation capacity of the conventional tubular brace increased 1.46 times due to the proposed design. The main conclusion of this research is that polyoxymethylene is a highly suitable material for the production of steel tubular buckling controlled braces.

Keywords: polyoxymethylene (POM); composite brace; buckling; cyclic loading; finite elements

1. Introduction

Concentrically braced frames (CBFs) are the most widely used lateral force resisting systems due to their relatively high lateral stiffness as well as their inexpensive fabrication and erection costs. In addition, tensile yielding and global buckling of brace elements in CBFs were taken into account as an energy dissipation mechanism. CBFs, however, have limited ability to dissipate energy due to buckling induced pinched hysteretic response. Moreover, unsymmetrical hysteretic behavior and local buckling-induced premature fractures of the bracing members inhibit the use of CBFs as a lateral system in a region of high seismicity.

Aforementioned performance issues have forced researchers to improve the seismic performance of braced frames. The attempt to improve the seismic performance of braced frames has resulted in many forms of lateral force resisting systems such as buckling restrained braces (BRBs) (Palazzo *et al.* 2009, Eryasar and Topkaya 2010, Hoveidae and Rafezy 2011, Tabatabaei *et al.* 2014, Moradi and Arwade 2014, Judd *et al.* 2016, Hosseinzadeh and Mohebi 2016, Shen *et al.* 2016, Mirtaheri *et al.* 2017, Mirtaheri *et al.* 2018, Hemati *et al.* 2018, Razaevi *et al.* 2018,), energy dissipater braces (Demir and Husem 2018, Aghlara and Tahir 2018, Aghlara *et al.* 2018), shape memory alloy braces (Asgarian and Moradi 2011) and tension only braces (Husem *et al.* 2016). From these lateral load resisting systems, concrete-encased BRBs provide a desirable seismic performance with their notable energy dissipation capacity and symmetrical hysteretic behavior. The heaviness and complicated structure of concrete-encased BRBs, however, along with the higher costs, limit their widespeared application. Thus, over the last decade, researchers turned their attention to all-steel buckling controlled braces (BCBs) instead of concrete-encased BRBs (Eryasar and Topkaya 2010, Hoveidae and Rafezy 2011, Judd *et al.* 2016, Hosseinzadeh and Mohebi 2016, Shen *et al.* 2016, Mirtaheri *et al.* 2017, Hemati *et al.* 2018). Similar to concrete-encased BRBs, an all-steel BCB is composed of a yielding steel core and of several steel sections that perform as a buckling controller. All-steel BCBs divided into two groups are named sandwiched plate BCBs (SP-BCBs) (Eryasar and Topkaya 2010, Hoveidae and Rafezy 2011, Judd *et al.* 2016, Mirtaheri *et al.* 2017) and steel tubular BCBs (ST-BCBs) (Hosseinzadeh and Mohebi 2016, Shen *et al.* 2016, Hemati *et al.* 2018). SP-BCBs have a complicated design, which often requires closely spaced bolted or welded attachments as well as cross sections that consist of a combination of plates and structural shapes. On the other, hand ST-BCBs are simple, practical and cost-effective since they significantly reduce the cost of labor. In addition, ST-BCBs avoid the use of complicated cross-sections and connections by removing bolts and welds from the construction process. ST-BCBs have very limited design opportunities in their current design method, however, due to only a few steel tubes, encased within each other, currently existing in the steel industry.

In this study, a new and practical design method is proposed in order to provide a widespeared application opportunities for current ST-BCBs applications.

2. Steel-polyoxymethylene composite brace concept

Traditionally, a ST-BCB system consists of a load bearing brace encased in another steel tube that acts as the

*Corresponding author, Ph.D.
E-mail: s.demir@ktu.edu.tr

http://www.techno-press.com/journals/sem&subpage=7
ISSN: 1225-4568 (Print), 1598-6217 (Online)

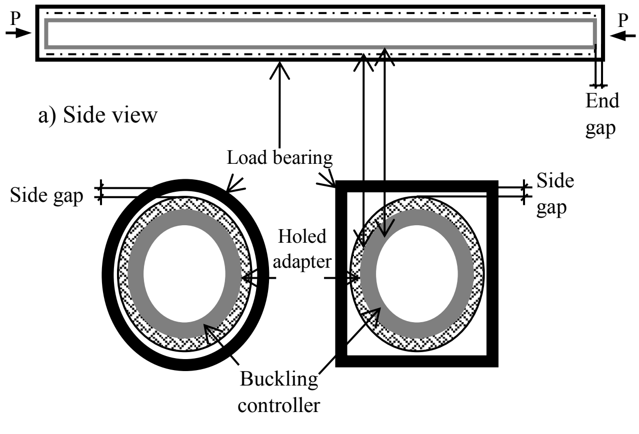

Fig. 1 Schematic view of the BCCBs

buckling controller. Therefore, there must be a gap between the load bearing brace and buckling controller to allow for the inside tube to slide freely. It is essential that, for proper application, the gap clearance and friction forces between tubes have very important effects on the cyclic behavior of the system. Studies have indicated that keeping the gap and friction contact between the load bearing brace and buckling controller as small as possible will result in optimal performance (Shen *et al.* 2016). Nevertheless, there is a very limited amount of steel tubes encased within each other, with smallest possible gap clearance, that exist in the steel industry. Therefore, in order to use all round and square tubes with smallest gap clearance possible, a simple and practical design method is proposed.

A buckling controlled composite brace (BCCB) system consists of a load bearing brace (outer tube), buckling controller (inner tube) and a holed-adapter used between them (Fig. 1). Unlike the ST-BCB, the buckling controller is used inside the load bearing brace in BCCBs. End gaps are left at both ends of the system to prevent the buckling controller tube's and the holed-adapter's contribution to axial load carrying capacity. The holed-adapter is used to fill the gap between the tubes. Polyoxymethylene is the preferred choice for the holed-adapter. Polyoxymethylene, also known as polyacetal, acetal, and polyformaldehyde, is an engineering thermoplastic used in precision parts requiring high stiffness, low friction, and excellent dimensional stability. Polyoxymethylene can either be easily manipulated by lathe to achieve the desired diameter or it can be cast into the needed shape.

2.1 Design procedure

The buckling load of a BCCB can be estimated by using the Euler buckling theory. The load bearing brace will buckle when the axial compression load, P, reaches the Euler buckling load. If the axial compression load continues to increase, an unknown distributed interaction load, q(x), will be generated along the load bearing brace. The unknown distributed interaction load is the transverse reaction of the buckling controller/holed-adapter along the load bearing brace. Fig. 2(a) shows the schematic of a BCCB in axial compression, while Figs. 2(b)-(c) show the unknown distributed interaction load on the load bearing brace and the buckling controller tube/holed-adapter in a deformed configuration. The equilibrium of the load bearing brace and buckling controller/holed-adapter in their deformed shape can be expressed with Eq. (1) and Eq. (2), respectively (Black *et al.* 2002):

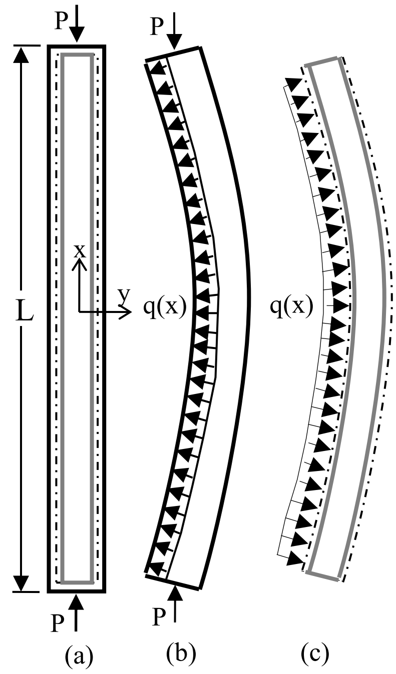

Fig. 2 BCCB under axial compression loading (a), unknown distributed interaction load along the load bearing steel tube (b) and bucking controller/holed-adapter (c)

$$E_b I_b \frac{d^4 y(x)}{dx^4} + P \frac{d^2 y(x)}{dx^2} = -q(x) \tag{1}$$

$$E_c I_c \frac{d^4 y(x)}{dx^4} + E_h I_h \frac{d^4 y(x)}{dx^4} = q(x) \tag{2}$$

where y(x) is transverse deflection, P is the axial compression load and E_bI_b, E_cI_c and E_hI_h are flexural rigidities of the load bearing brace, buckling controller and holed-adapter, respectively. If the unknown distributed interaction load, q(x), is eliminated by equating Eq. (1) and Eq. (2), a homogeneous Euler equation will result:

$$\frac{d^4 y(x)}{dx^4} + \frac{P}{E_b I_b + E_c I_c + E_h I_h} \frac{d^2 y(x)}{dx^2} = 0 \tag{3}$$

For a brace with buckling length, L, Eq. (3) yields the critical buckling load, P_{cr}, of the brace as:

$$P = P_{cr} = \frac{\pi^2}{(KL)^2} (E_b I_b + E_c I_c + E_h I_h) \tag{4}$$

where KL is the effective length. Finally, global stability of the BCCB is ensured when the critical buckling load, P_{cr}, exceeds the yielding load, P_y, of the load bearing brace:

$$P_{cr} > P_y = \sigma_y A_b \qquad (5)$$

3. Experimental studies

3.1 Material properties

Three tensile test coupons of the S355JR steel used in the production of the load bearing brace and buckling controller were prepared in accordance with ASTM A370-13 (2010), followed by a uniaxial tensile test (Fig. 3). The overall length of the coupon specimens was 170 mm, with 40 mm long by 35 mm wide grip sections at each end. The reduced section had a nominal width equal to 15 mm and a length equal to 90 mm. A strain gauge with a 60 mm length was used on the reduced section to obtain strain values. The mechanical properties of the holed-adapter (polyoxymethylene rod) were provided by manufacturer. The average mechanical properties of the materials are summarized in Table 1.

Fig. 3 Uniaxial tensile test

Table 1 Average mechanical properties of the materials

Section	Elastic modulus (GPa)	Yield strength (MPa)	Tensile strength (MPa)	Elongation (%)
Load bearing brace	196.1	386.5	449.4	26.7
Buckling restrainer	198.7	364.6	437.1	24.2
Holed adapter*	3.0	72	67	17

*Holed adapter: Provided by manufacturer

3.2 Test specimens and fabrication

Two test specimens were fabricated to investigate the types of behavior seen under displacement controlled cyclic loading. The dimensions of the specimens are presented in Fig. 4. The first specimen, named CB, is represents the conventional braces, which are commonly used in steel structures. CB consists of a round HSS 76.1x2.5 mm load bearing brace with pinned connection members at each end. The total length of the brace and entire assemble (from pin to pin) are 1740 mm and 2000 mm, respectively. The second specimen, named BCCB, represents the buckling controlled composite braces proposed in this study. BCCB consists of a round HSS 76.1x2.5 mm load bearing brace, a round hollow 70x13.8 mm holed-adapter, a round HSS 42.4x4.0 mm buckling controller along with pinned connection members at each end (Fig. 5). The total length of the brace, holed-adapter, buckling controller and entire assemble (from pin to pin) are 1740 mm, 1710mm, 1710 mm and 2000 mm, respectively. The diameter of the holed-adapter was adjusted with lathe and a 1 mm gap left between holed adapter and load bearing brace. All steel connections were made by fillet weld using E70 type electrodes.

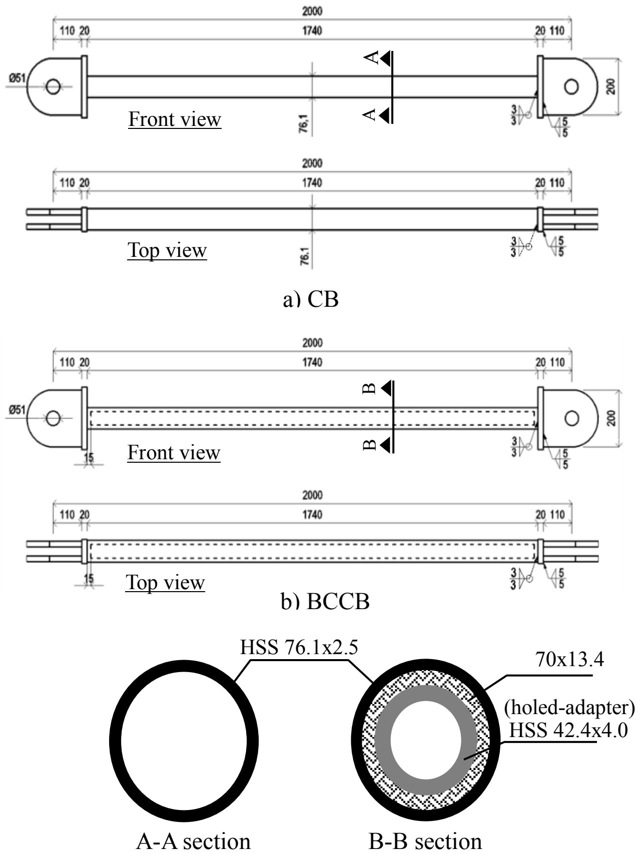

Fig. 4 Dimensions of the test specimens (mm)

3.3. Test setup, instrumentation and loading protocol

Fig. 6 shows the test setup, which was designed to simulate the loading, deformations and end connections expected in a framing system. Horizontal displacement was applied via hydraulic actuator with a force capacity of 350 kN, and a maximum stroke length equal to 200 mm. The bottom end of the rigid column acts as a true pin (50-mm diameter pin and 15-mm thick plates) while the rigid beam is bolted to the strong floor. A lateral support was installed to restrain out-of-plane movement of the rigid column. The 2*IPE200 column of the test setup was 1395 mm long from loading point to pinned base. To minimize the column deformations, sufficiently stiff column size was selected. The test specimens were connected to the 35 mm thick gusset plates using 50 mm diameter pins.

Test specimens were subjected to quasi-static displacement, described in Table 2, that were derived from buckling restrained brace design provisions found in K3 in

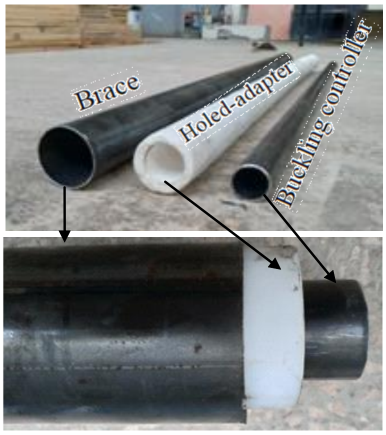

Fig. 5 Preparation of BCCB specimen

Table 2 Loading history

Number and amplitude of cycles (mm)	Cycle	Pick deformation
2 @ 2.00	1,2	< δby
2 @ 4.00	3,4	Δby
2 @ 13.95	5,6	0.5δbm
2 @ 27.90	7,8	1.0 δbm
2 @ 41.85	9,10	1.5 δbm
2 @ 55.80	11,12	2.0 δbm
2 @ 41.85	13,14	1.5 δbm

AISC 341-10 (2010). The loading history consists of two cycles at deformation, corresponding to the critical buckling load of the test specimen, δ_{by}, followed by two cycles each at peaks of 0.5, 1.0, 1.5, and 2.0 times the design story drift deformation, δ_{bm}. Design story drift was accepted as 0.02, which is the upper limit as outlined by ASCE 7-10 (2010). The displacement at critical buckling, δ_{by}, was determined via finite element analysis, is described in the next section.

4. Numerical study

Three-dimensional nonlinear finite element analysis was conducted using Ansys software. Material properties were defined by element type, material model and key options. The load bearing brace, holed-adapter and buckling controller were modeled using Solid185, 8-node tetrahedral element, which has stress stiffening, large deflection and large strain capabilities along with having three degrees of freedom at each node: transition in the nodal x, y and z directions. Multi point constraint elements (MPC184) are used to simulate the boundary conditions of the specimens (Fig. 7). To do this, master nodes were identified at the center of each pinned end and were then connected to nodes at the edges of the brace by MPC184. Displacement of the first master node was restrained in all directions while rotation around the z axis unrestrained. Similarly, the displacement of the second master node was restrained in the y and z directions, while transition in the x direction and rotation around the z axis were unrestrained. Multilinear kinematic hardening models were used, which included the Bauschinger effect in order to model the metal plasticity behavior under cyclic loading.

The interaction between the load bearing brace and holed-adapter was modeled using contact elements.

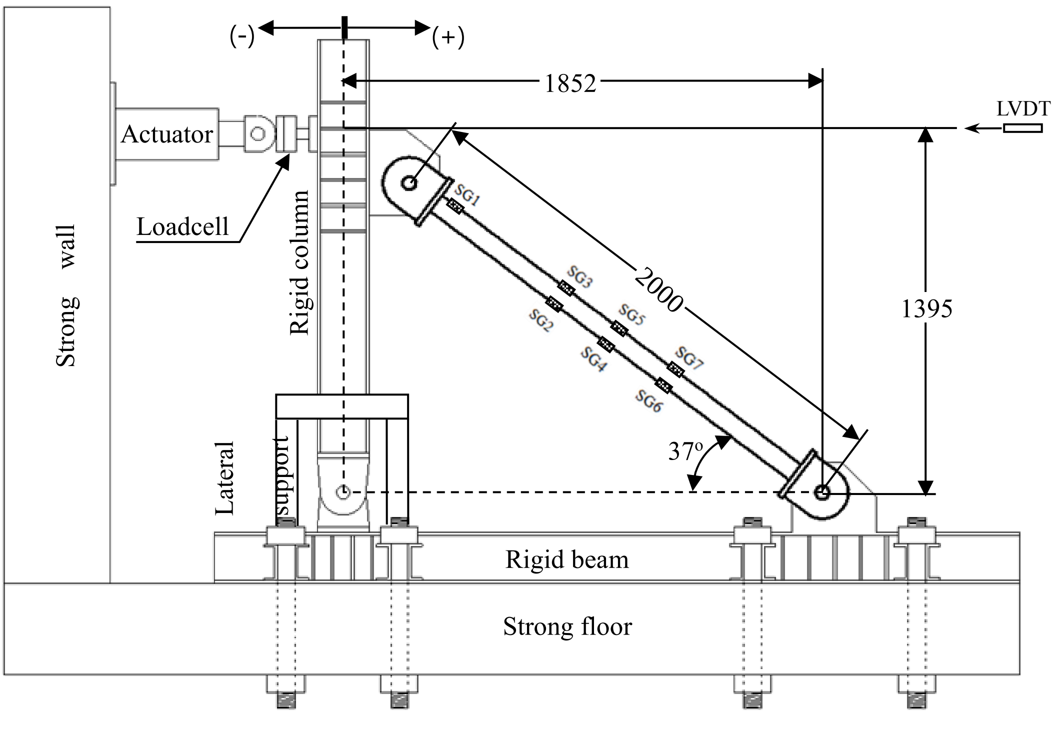

Fig. 6 Test setup

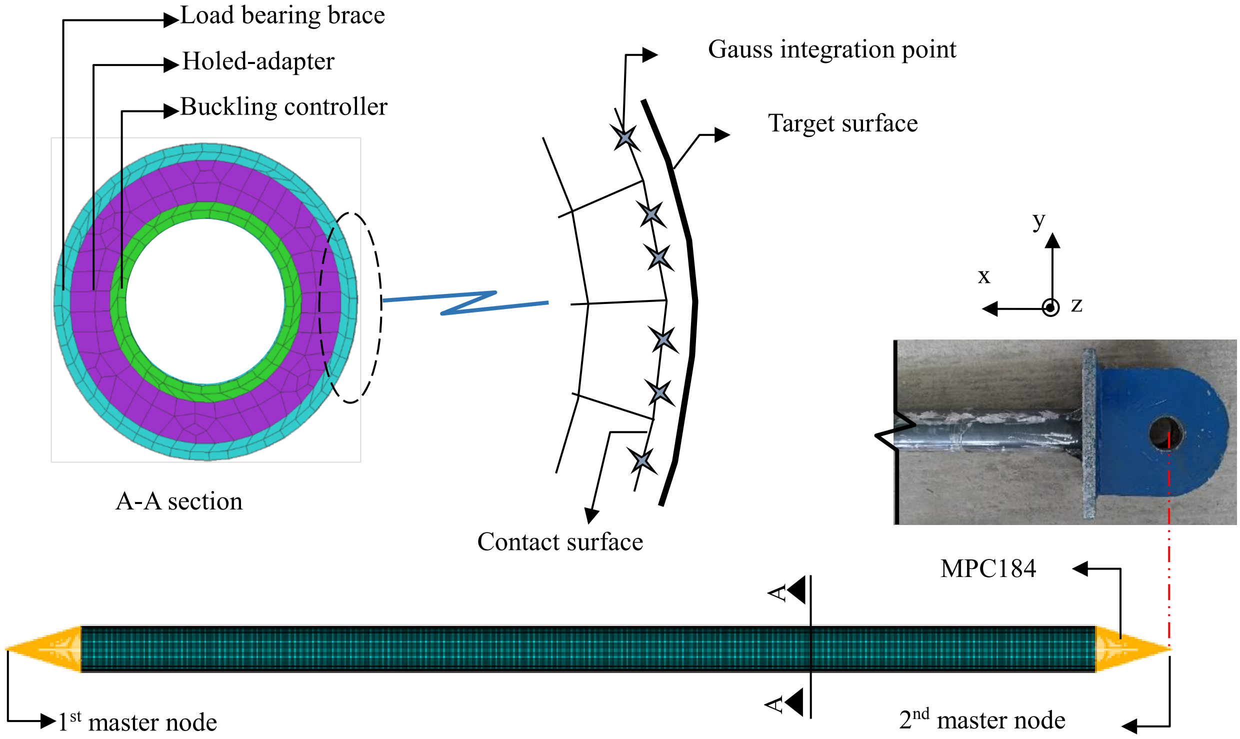

Fig. 7 Finite element model for BCCB

A surface-to-surface contact algorithm was selected to simulate the contact mechanism between the reciprocal surfaces of these two different materials. Due to greater rigidity, the target surface was selected as the inner surface of the load bearing brace while the outer surface of the holed-adapter acted as the contact surface (Fig. 7). The contact status between these two surfaces was regularly determined at Gauss integration points. In accordance with the chosen contact behavior, local separation of the surfaces is allowed, while, normal pressure equals zero if separation occurs.

Finally, a quasi-static analysis was performed and the full Newton-Raphson method was used for the nonlinear analysis. For displacement controlled cyclic loading a total of 52 load steps were defined. All loads steps were divided into multiple sub-steps until the total load was achieved.

5. Results and discussions

5.1 Experimental results

The hysteresis responses and backbone curves of the test specimens obtained from experimental studies are shown in Figs. 8. In addition, yield load (P_y), yield displacement (δ_y), initial stiffness (k), drift ratio (Δ) and maximum load (P_{max}) are summarized in Table 3.

The CB specimen showed a typical conventional brace behavior during the cyclic loading test (Fig. 10). At the 4.57 mm horizontal displacement (5th cycle), the CB specimen reached to a 131.9 kN yield load first followed by global buckling. Therefore, a sudden decrease in the load carrying response happened at the end of the compression loading of the 5th cycle. In each tensile yielding cycle the CB specimen is plastically elongated, meaning the yield displacement of the member increases in each cycle. This caused the hysteresis to drift towards the tension displacement side, as shown in Fig. 8. Moreover, the elongation of the brace in each tensile cycle resulted in decreased buckling resistance of the member and pinching of the hysteresis in each subsequent inelastic compression cycle. During the 7th cycle, local buckling was observed at the center of the brace. After several cycles, the plastic hinge region at the centre of the brace accumulated damage, leading to further pinching of the hysteresis and a reduction in the load carrying capacity. During tension loading of the 9th cycle (41.85 mm displacement level) tear-through failure occurred at the center of the brace. Fig. 10 illustrates the failure mode results.

The BCCB specimen showed an improved cyclic performance relative to the CB specimen (Fig. 8). At the 4.78 mm horizontal displacement (5th cycle), the BCCB specimen reached a 142.1 kN yield load. Continuation of the same loading cycle brace section completely plasticized and reached a maximum load at 157.1 kN with a 12.28 mm displacement level (0.88 % drift). Brace buckling had been controlled until this point. Load response decreased from 157.1 to 108.7 kN. In each tensile loadings, the BCCB specimen showed similar behavior to the CB specimen precisely because the buckling controller and holed-adapter have no contribution on tensile force.

After each tensile loading, the BCCB specimen showed an improvement in buckling resistance, in comparison to the CB specimen, with the contribution of the buckling controller and holed-adapter. This contribution, however, did result in cracking noises from the holed-adapter

Table 3 Results summary

Specimen		Yield load									
		Positive loading (+)					Negative loading (-)				
		P_y (kN)	δ_y (mm)	Δ (%)	k (kN/mm)	P_{max}/P_y	P_y (kN)	δ_y (mm)	Δ (%)	k (kN/mm)	P_{max}/P_p
CB	**Exp.**	131.9	4.57	0.33	28.90	1.0	-162.7	-5.12	0.37	31.8	1.04
	Num.	118.3	3.11	0.22	38.03	1.0	-149.7	-5.01	0.36	29.9	1.15
BCCB	**Exp.**	142.1	4.78	0.34	29.70	1.11	-151.3	-4.75	0.34	31.8	1.12
	Num.	180.2	4.16	0.30	43.32	1.01	-180.3	-4.45	0.32	40.51	1.01

Specimen		Max. load					
		Positive loading (+)			Negative loading (-)		
		P_{max} (kN)	δ (mm)	Δ (%)	P_{max} (kN)	δ (mm)	Δ (%)
CB	**Exp.**	131.9	4.63	0.33	-169.3	-28.1	2.01
	Num.	118.3	3.11	0.22	-171.7	-27.9	2.00
BCCB	**Exp.**	157.1	12.28	0.88	-169.3	-27.7	1.99
	Num.	181.4	41.0	2.94	-181.26	-30.0	2.15

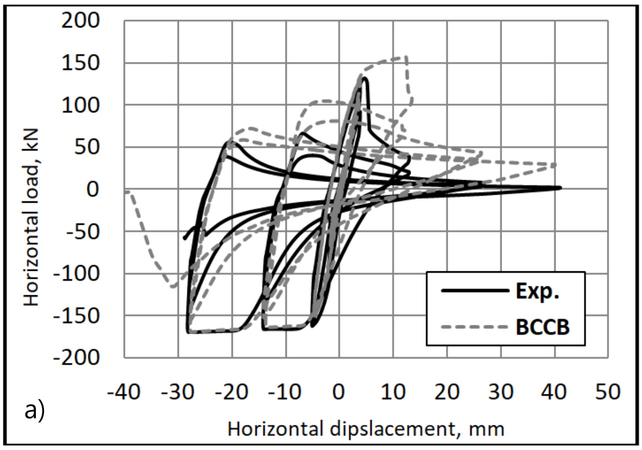

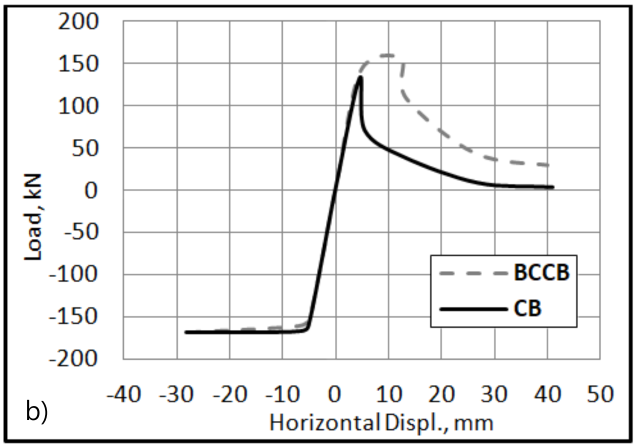

Fig. 8 a) Hysteresis responses and b) backbone curves of the specimens

throughout the experiment (Fig. 12). During the 7th cycle, local buckling was observed at the approximate center of the brace. After several cycles, the plastic hinge region at the centre of the brace accumulated damage. During the tension loading of the 9th cycle (41.85 mm displacement level) tear-through failure occurred at the approximate center of the brace. Fig. 11 shows the failure mode obtained during the tests.

5.1.1 Energy dissipation capacity and equivalent stiffness

Seismic performance of a brace is often measured by the energy dissipated because during a strong ground motion the elastic capacity of the braces will be exceeded and the dynamic behavior must be controlled through energy dissipation. Conventional braces have limited ability to dissipate energy. However, energy dissipation of a conventional brace can be enhanced with composite brace design as suggested in this study.

The energy dissipated by the test specimens was calculated according to area under the hysteretic curves at a particular displacement level. Since each displacement cycle was repeated two times, the total energy dissipated by a specimen at any displacement cycle can represent the cumulative energy dissipation value. The energy dissipation capacity of the specimen is increased exponentially with the rise of displacements. Both test specimens dissipated almost the same amount of energy until yielding load level (4th cycle). After this load level, test specimens showed different energy dissipation mechanisms under compressive loads as well as differences between dissipated cumulative energy values (Fig. 13). The buckling induced bending behavior of the buckling controller and holed-adapter improved the energy dissipation capacity of the BCCB specimen. As a result, BCCB dissipated energy 1.46 times higher than CB. The total value of energy dissipated by the specimens CB and BCCB are calculated as 13.8 and 20.2 kJ, respectively.

Equivalent stiffness of the test specimens are shown in Fig 13. Note that, Fig. 8(a) is drawn according to compression loadings only. Both test specimens showed approximately the same initial stiffness in the elastic range. This result shows the low friction feature of the holed-

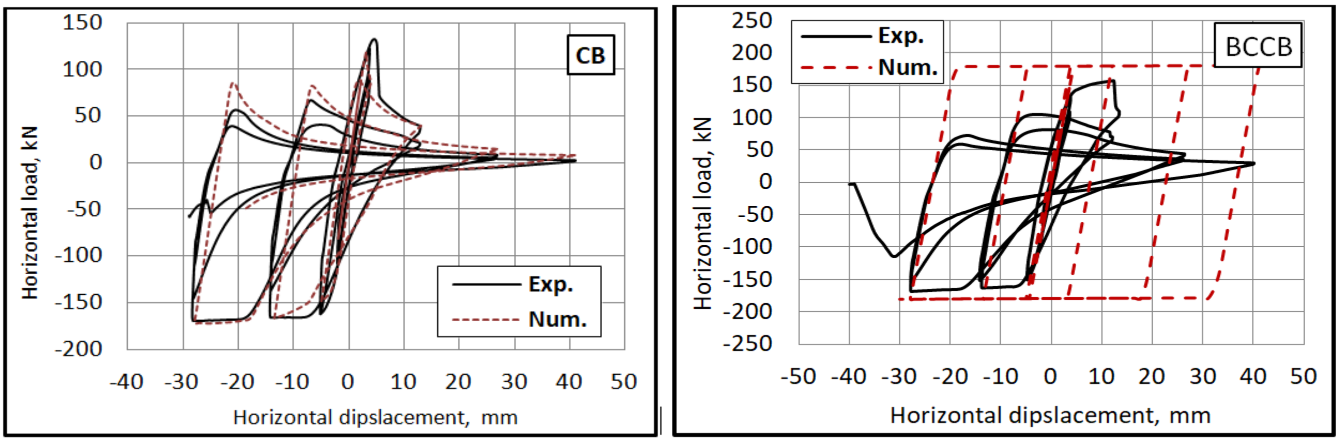

Fig. 9 Experimental and numerical hysteresis curves of the specimens

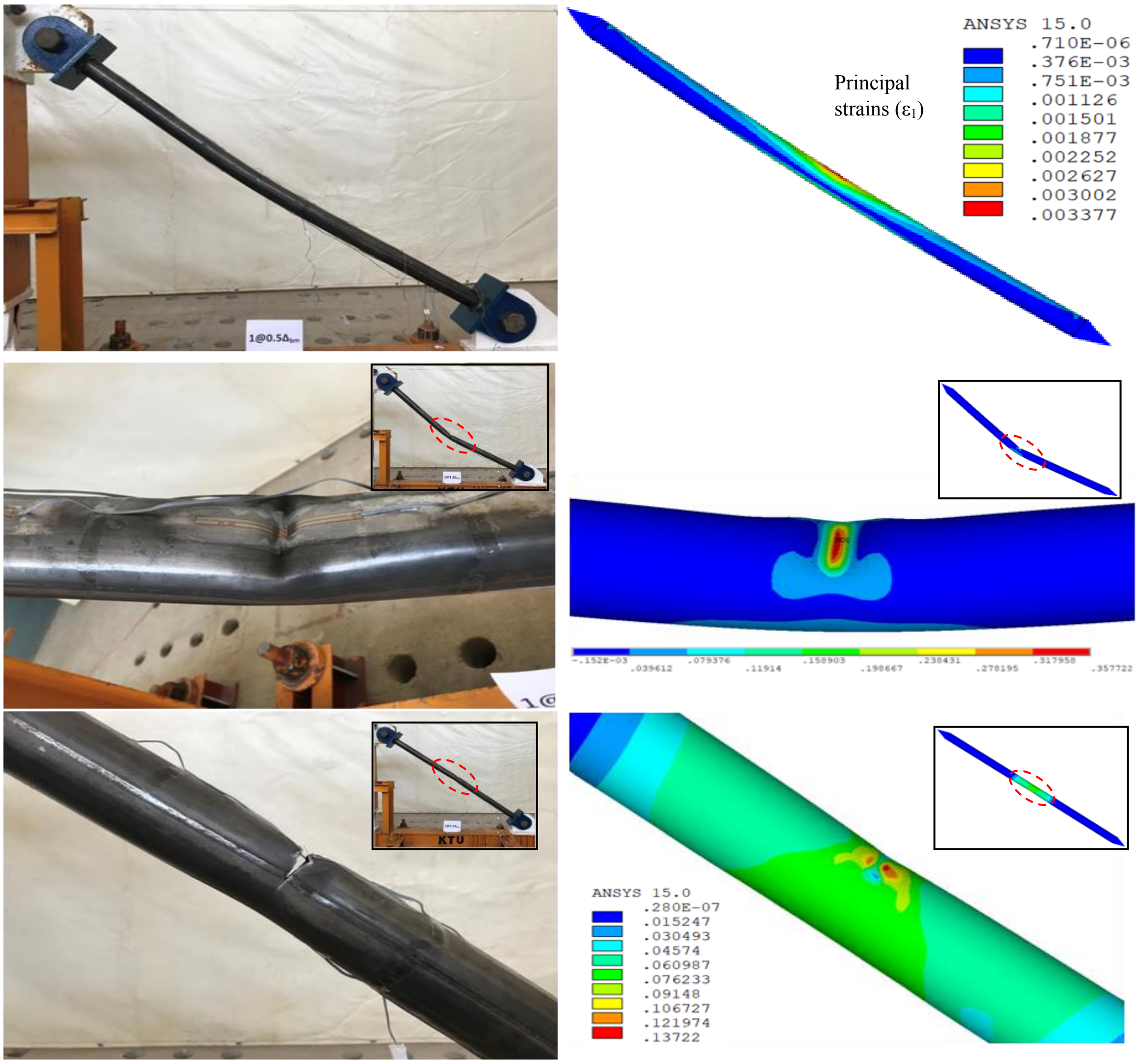

Fig. 10 Buckling behavior of CB

adapter has not had a significant effect on the initial stiffness. After the yielding load, both test specimens showed rapid strength loss while equivalent stiffness was evaluated as 2.87 and 8.1 kN/mm for the CB and BCCB specimens, respectively. Therefore, the holed-adapter and buckling controller provide anincrease in stiffness to the brace, after buckling.

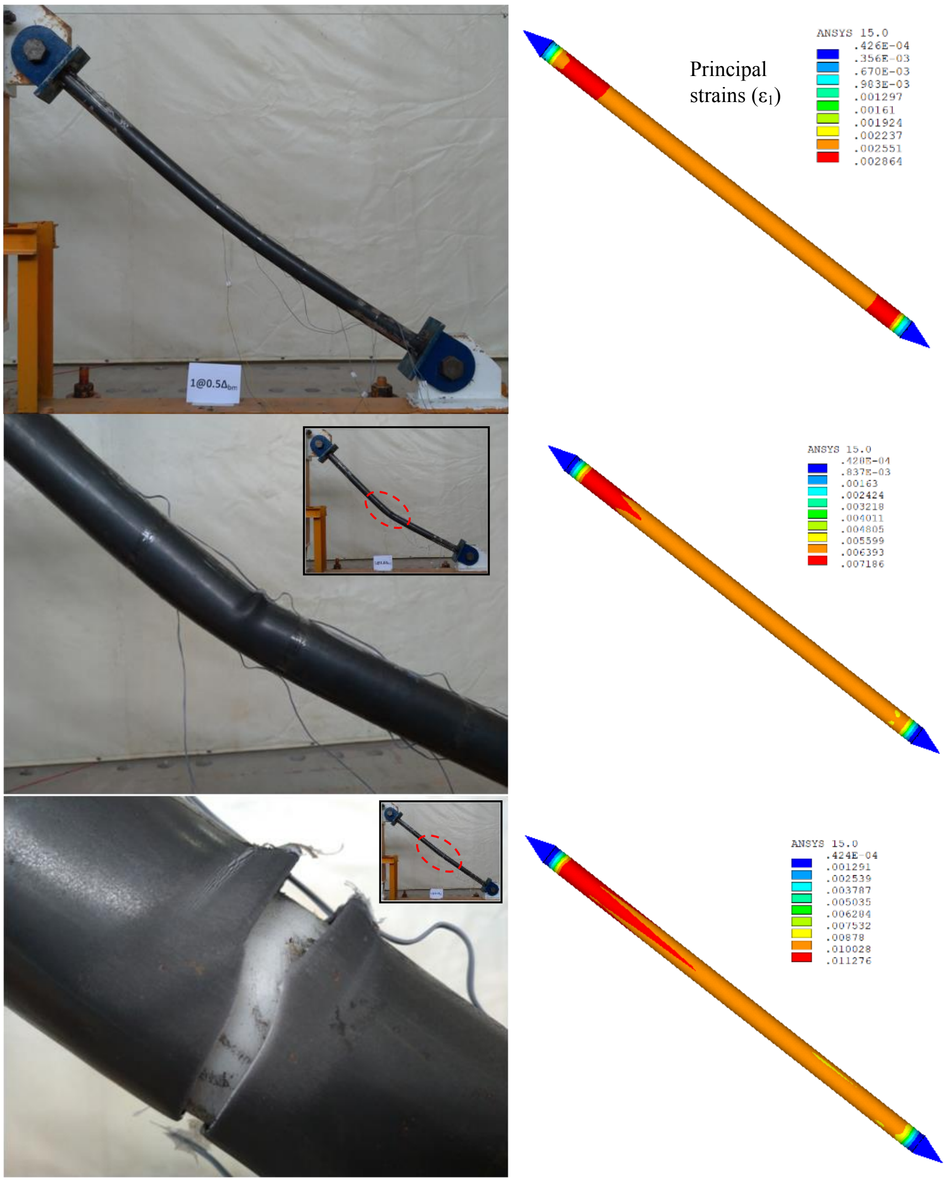

Fig. 11 Cyclic behavior of BCCB

5.1.2 Strain distribution patterns

In the both specimens strain distribution until global buckling was uniform along the brace length (Fig. 14). This uniform strain distribution was lost, however, for the CB specimen at a 4.57 mm displacement (beginning of the 5th cycle) while the BCCB specimen kept uniform strain distribution until a 12.28 mm displacement (end of the 5th cycle). After global buckling, large strains were recorded at SG3, SG4 and SG5 in CB while at SG2,SG3, SG4, SG5, SG6 and SG7 were seen in BCCB (Fig 14). Evidence clearly shows how, more strains are concentrated at the midsection of the BCCB specimen. This difference between the strain distributions of the specimens is due to the buckling conditions. Buckling only slowly occurred in the CB specimen while it occurred very rapidly in the BCCB specimen precisely because of the cracking of the holed-adapter from the mid-point. In the following cycles, local buckling occurred in the midsection and the strains became concentrated around the midsection of the specimens. Finally, fracturing occurred at the midsection of the specimens after severe local buckling. According to the strain results, the BCCB specimen recorded greater strain values, however, this situation did not make a difference on the fracture life of the specimens.

5.2 Numerical results

The hysteresis responses of the test specimens obtained from numerical studies are shown in Figs. 9, 10 and 11. Numerical results of the CB specimen showed a good agreement with the experimental results in terms of the hysteretic behavior and buckling mode. In the experimental study, the buckling load was 131.9 kN at a 4.57 mm displacement, while in the numerical study the buckling

Fig. 12 Damage mode of holed-adapter (end of test)

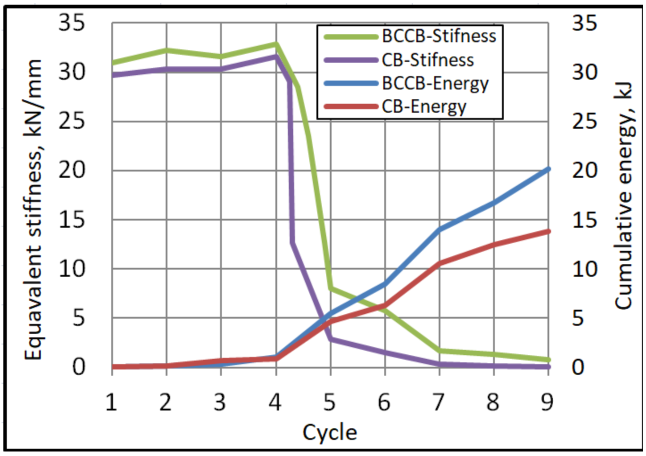

Fig. 13 Energy dissipation and equivalent stiffness curves

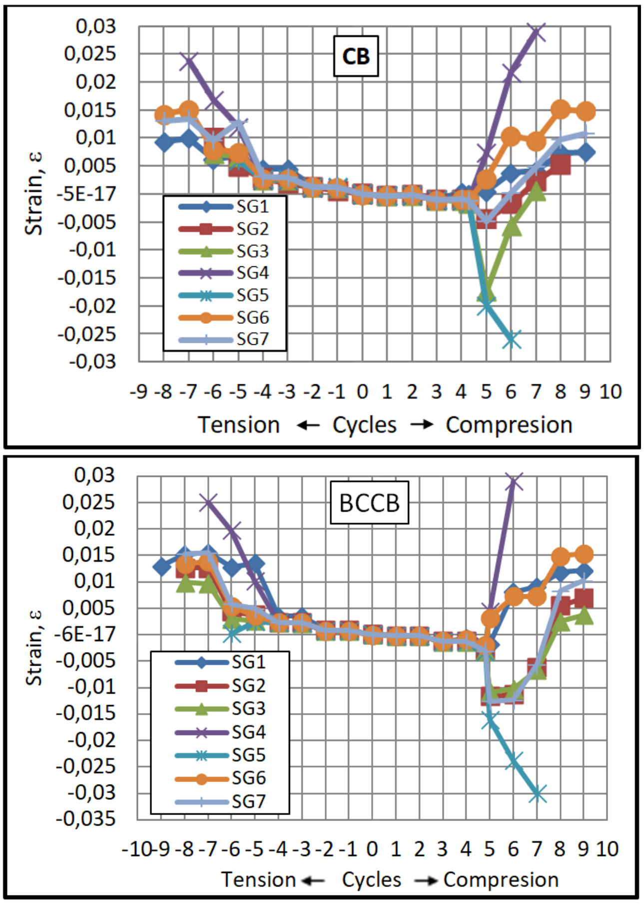

Fig. 14 Strain distribution patterns

load was 118.3 kN at a 3.11 mm displacement. Between the experimental and numerical results 11.4% and 46.9% errors were calculated for buckling load and displacement, respectively. The error of 46.9 % is a direct result from slight slackness at the pinned connections. During the following cycles local buckling and damage concentration were well predicted in the numerical study (Fig 10).

The hysteresis response of the BCCB specimen was not exactly predicted in the numerical study (Fig 9). In the experimental study, the yield load was 142.1 kN at 4.78 mm displacement, while in the numerical study the yield load was 180.2 kN at 4.16 mm displacement. Between the experimental and numerical results, 21.1% and 14.9% errors calculated for yield load and displacement. However, buckling happened a 12.28 mm displacement level in the experimental study but did not occured in numerical study. Therefore, the buckling load was not predicted for the BCCB specimen in numerical study in part due to the sudden cracking of the holed-adapter, which was not simulated correctly.

6. Conclusion

In this paper, the design and cyclic behavior of a simple and practical buckling controlled composite brace system are presented. Experimental and numerical studies of the test specimens were carried out and the following conclusions were made:

- The holed-adapter and buckling controller kept the stability of the conventional brace while also provided buckling control until the 0.88 % drift ratio. These features of the system can play an important role in reducing early damage concentration to the braces. The proposed system also showed better energy dissipation capacity relative to the conventional brace.
- Owing to the low friction capacity of the holed-adapter, initial stiffness of the system did not change in the elastic zone but yield load did increased relative to the conventional brace. This feature of the system gives an opportunity to engineers to design the system in the same way as the conventional braces.
- The decrease in the rate of strength loss per cycle, improvement of ductility and the increase in energy dissipation capacity are the direct results of using a holed-adapter, which is an efficient way to improve the seismic performance of conventional tubular braces.
- The proposed system did not improved axial deformation capacity of the conventional brace and both fractured until a drift ratio of 3 %.
- A safety factor can be taken into consideration in Eq. (4) to explore the possibility of further delaying the buckling.
- As this study relied on the use of polyoxymethylene,

the effects of other engineering polymers, like polyamide (Nylon6.6), on the behavior of conventional tubular braces should be investigated in future studies.

References

Aghlara, R. and Tahir, M.Md. (2018), "A passive metallic damper with replaceable steel bar components for earthquake protection of structures", *Eng. Struct.*, **159**, 185-197. https://doi.org/10.1016/j.engstruct.2017.12.049.

Aghlara, R., Tahir, M.Md. and Adnan, A.B. (2018), "Experimental study of pipe-fuse damper for passive energy dissipation in structures", *J. Construct. Steel Res.*, **148**, 351-360. https://doi.org/10.1016/j.jcsr.2018.06.004.

ANSI/AISC 341–10 (2010), Seismic Provisions for Structural Steel Buildings, American Institute for Steel Construction; Chicago, IL, USA.

Ansys (2015), Swanson Analysis System, USA.

ASCE/SEI 7–10 (2010), Minimum Design Loads for Buildings and Other Structures, American Society of Civil Engineers; Reston, VA, USA.

Asgarian, B. and Moradi, S. (2011), "Seismic response of steel braced frames with shape memory alloy braces", *J. Construct. Steel Res.*, **67**, 65-74. https://doi.org/10.1016/j.jcsr.2010.06.006.

ASTM A370-13 (2010), Standard Test Methods and Definitions for Mechanical Testing of Steel Products, American Society for Testing and Materials; West Conshohocken, PA, USA.

Black, C., Makris, N. and Aiken, L. (2002), "Component testing, stability analysis characterization of buckling-restrained unbonded braces", Research Report No. PEER 2002/08; Pacific Earthquake Engineering Research Center, USA.

Demir, S. and Husem, M. (2018), "Saw type seismic energy dissipaters: development and cyclic loading test", *J. Construct. Steel Res.*, **150**, 264-276. https://doi.org/10.1016/j.jcsr.2018.08.015.

Eryasar, M.E. and Topkaya, C. (2010), "An experimental study on steel-encased buckling-restrained brace hysteretic dampers", *Earthquake Engng Struct. Dyn.*, **39**, 561-581. https://doi.org/10.1002/eqe.959.

Hemati, S.A., Bafghi M.A.B. and Kheyroddinc, A. (2018), "Experimental investigation of pod on the behavior of all-steel buckling restrained braces", *J. Construct. Steel Res.*, **150**, 186-194.

Hosseinzadeh, Sh. and Mohebi, B. (2016), "Seismic evaluation of all-steel buckling restrained braces using finite element analysis", *J. Construct. Steel Res.*, **119**, 76-84. https://doi.org/10.1016/j.jcsr.2015.12.014.

Hoveidae, N. and Rafezy, B. (2012), "Overall buckling behavior of all-steel buckling restrained braces", *J. Construct. Steel Res.*, **79**, 151-158. https://doi.org/10.1016/j.jcsr.2012.07.022.

Husem, M., Demir, S., Park, H.G. and Cosgun, S.I. (2016), "Diagonal bracing of steel frames with multi-cable arrangements", *Struct. Eng. Mech.*, **59**(6), 1121-1136. https://doi.org/10.12989/sem.2016.59.6.1121.

Judd, J.P., Marinovic, I., Eatherton, M.R., Hyder, C., Philips, A.R., Tola Tola, A. and Charney, F.A. (2016), "Cyclic tests of all-steel web-restrained buckling- restrained brace subassemblages", *J. Construct. Steel Res.*, **125**, 164-172. https://doi.org/10.1016/j.jcsr.2016.06.007.

Mirtaheri, S.M., Nazeryan, M., Bahrani, M.K., Nooralizadeh, A., Montazerian, L. and Naserifard, M. (2017), "Local and global buckling condition of all-steel buckling restrained braces", *Steel Compos. Struct.*, **623**(2), 217-228.

Mirtaheri, M., Sehat, S. and Nazeryan, M. (2018), "Improving the behavior of buckling restrained braces through obtaining optimum steel core length", *Struct. Eng. Mech.*, **65**(4), 401-408. https://doi.org/10.12989/sem.2018.65.4.401.

Moradi, M. and Arwade, S.R. (2014), "Improving buckling response of the square steel tube by using steel foam", *Struct. Eng. Mech.*, **51**(6), 1017-1036. https://doi.org/10.12989/sem.2014.51.6.1017.

Palazzo, G., López-Almansa, F., Cahís, X. and Crisafulli, F. (2009), "A low-tech dissipative buckling restrained brace. Design, analysis, production and testing", *Eng. Struct.*, **91**, 2152-2161. https://doi.org/10.1016/j.engstruct.2009.03.015.

Razavi, S.A., Kianmehr, A., Hosseini, A. and Mirghaderi, S.R. (2018), "Buckling-restrained brace with CFRP encasing: Mechanical behavior & cyclic response", *Steel Compos. Struct.*, **27**(6), 675-689. https://doi.org/10.12989/scs.2018.27.6.675.

Shen, J. Seker, O., Sutchiewcharn, N. and Akbas, B. (2016), "Cyclic behavior of buckling-controlled braces", *J. Construct. Steel Res.*, **121**, 110-125. https://doi.org/10.1016/j.jcsr.2016.01.018.

Tabatabaei, S.A.R., Mirghaderi, S.R. and Hosseini, A. (2014), "Experimental and numerical developing of reduced length buckling-restrained braces", *Eng. Struct.*, **77**, 143-160. https://doi.org/10.1016/j.engstruct.2014.07.034.

CC